Biomass and Bioenergy 122 (2019) 381–390

Contents lists available at ScienceDirect

Biomass and Bioenergy

journal homepage: www.elsevier.com/locate/biombioe

Research paper

Pyrolytic temperature evaluation of macauba biochar for uranium adsorption from aqueous solutions

S.N. Guilhen[a,*], O. Mašek[b], N. Ortiz[a], J.C. Izidoro[a], D.A. Fungaro[a]

[a] Centro de Química e Meio Ambiente, Instituto de Pesquisas Energéticas e Nucleares, Av. Prof. Lineu Prestes 2242 - Cidade Universitária, 05508-000, São Paulo/SP, Brazil
[b] UK Biochar Research Centre, University of Edinburgh, School of Geosciences, Crew Building, Alexander Crum Brown Road, EH9 3LA, Edinburgh, UK

ARTICLE INFO

Keywords:
Biochar
Pyrolysis
Adsorption
Macauba
Uranium

ABSTRACT

This study aims to evaluate the effect of the pyrolytic temperature on the biochar derived from the macauba endocarp for the removal of uranium (VI) from aqueous solutions. The endocarp was subjected to six different pyrolytic temperatures, ranging from 250 °C to 750 °C. The biochars obtained at each temperature were evaluated for their adsorption capacities ("q"). The highest adsorption capacities were obtained for the biochar produced at 250 °C (BC250), followed by the one obtained at 350 °C (BC350), with removal efficiencies of 86% and 80%, respectively. The best condition was achieved when the endocarp was subjected to temperatures between 300 and 350 °C, at which it was possible to obtain a satisfactory balance among adsorption capacity, gravimetric yield and fixed carbon content. This characteristic, combined with the high removal efficiency, points to an ideal working temperature of 350 °C. Elemental analysis showed a decrease of the H/C and O/C ratios when higher pyrolytic temperatures were applied, indicating an inverse relationship between the carbonization and the surface polar functional groups, which were likely responsible for an increased adsorptive capacity in biochars produced at lower temperatures. Both FTIR and XPS analysis indicated that oxygen-containing groups such as hydroxyls and carboxylic acids were involved with the binding of uranyl ions.

1. Introduction

Radioactive wastes are generated in a variety of forms, states, concentrations and activities. The radionuclides present in radioactive waste can have a broad spectrum of half-lives. This is an indisputably complex problem, which often requires the combination of several techniques for its treatment and management [1].

Radioactive waste management is very important to safeguard human health and minimize the impact on the environment. Three general principles are employed in management of radioactive wastes before they can be harmlessly returned to the biosphere: concentrate-and-contain, dilute-and-disperse, delay-and-decay. Wastes can be concentrated and isolated, diluted to acceptable levels and discharged into the environment or stored until their radioactivity is allowed to naturally decrease through decay of the radioisotopes in them [2].

Safety management requires a number of operations and sometimes permanent containment. Treatment techniques may involve simple operations such as compaction to reduce volume, as well as advanced and/or complementary operations such as filtration, precipitation or ion exchange to remove the radionuclides from solutions. Once the waste is changed into a form that is suitable for safe handling, transportation, storage and disposal, it can be immobilized in suitable containers [3].

Nowadays, liquid radioactive wastes are generated as a result of many activities, such as mining and processing, the nuclear fuel cycle, nuclear medicine, industry and research [4]. Among the radionuclides commonly present in radioactive waste, uranium (U) can be of great concern due to its radiotoxicity. Naturally occurring isotopes of U decay by emission of alpha particles, which are highly ionizing. Since alpha particles are less penetrating than beta particles and gamma rays, they can be readily stopped by the skin or a sheet of paper, therefore not posing a great threat when exposure occurs outside of the body. However, the greatest radiological hazard would be when U is in close proximity to a cell or tissue, which would be possible through ingestion or inhalation (internal contamination). In this case, the alpha particles would be able to irradiate the body internally, sometimes, for a long period of time, initiating cell and tissue damage that could eventually lead to cancer. Of course, the severity of this contamination is related to the intensity of the irradiation source, which would depend on the degree of enrichment, the amount incorporated, the half-life, the affected organ or tissue, etc. [5].

An additional hazard is present in aquatic environments. Water

* Corresponding author.
E-mail address: snguilhen@ipen.br (S.N. Guilhen).

https://doi.org/10.1016/j.biombioe.2019.01.008
Received 29 January 2018; Received in revised form 20 December 2018; Accepted 21 January 2019
Available online 14 February 2019
0961-9534/ © 2019 Elsevier Ltd. All rights reserved.

chemistry alters uranium toxicity by changing its chemical form and, subsequently, its bioavailability [6]. Soluble species of uranium are more easily dispersed into water and can rapidly spread to the environment. Therefore, uranium contaminated wastes cannot be released in the wastewater without previous treatment.

New materials and processes are constantly being developed to improve decontamination and volume reduction in order to ensure safe storage and to decrease potential environmental impacts. In this regard, the use of sorbents has been growing over the years for they provide efficient and specific removal of contaminants from solutions [7]. The treatment of radioactive aqueous waste containing uranium comprises the reduction of volume through the separation of the radionuclide from the aqueous matrix, followed by its impregnation in the adsorbent. Once the activity levels in the aqueous waste are lowered to a safe level for liberation, the treated solution can be disposed of in the sewer system as industrial waste [8]. In Brazil, the regulation CNEN-NN-8.01 (2014) establishes the allowable limits [9] and the National Nuclear Energy Commission (CNEN) is responsible for monitoring and management of radioactive waste.

Immobilization of the adsorbent-adsorbate is required for long-term storage if its activity is above limits, serving as a barrier that prevents or slows the release of radionuclides into the environment. Cement, bitumen and polymers are usually employed as immobilization matrices, the selection of which depends on their chemical compatibility with the waste, commercial availability and costs [10,11]. In Brazil, the regulation CNEN-NN-6.09 “Acceptance criteria for radioactive waste disposal” [12], states that the radioactive solid waste must be immobilized in a matrix, so as to reduce the potential migration or dispersion of radionuclides.

Low-cost by-products from agricultural activities have been studied as a sustainable solution for wastewater treatment, as they can remove contaminants and pollutants from wastewater while at the same time contributing to waste reduction, recovery and reuse [13]. In recent years, there has been an increased interest in biochar, due to its many potential applications including carbon sequestration and enhancement of soil fertility [14], production of energy [15] and environmental remediation [16].

Biochar (BC) is a porous stable material, obtained from thermal degradation of carbon-rich biomass under an oxygen-limited atmosphere. Biochars typically exhibit great potential as adsorbent materials, mostly because of their porous structure, charged surface and surface functional groups. Several studies have demonstrated that biochars can be employed as low-cost wastewater treatment because they effectively remove heavy metals from aqueous solutions [17,18].

Among the array of biomass thermal conversion technologies, pyrolysis is a process in which organic matter is heated to temperatures above 300 °C in the absence of oxygen [19,20] with the aim to produce liquid and solid products. During the pyrolysis process, the natural polymeric constituents (lignin, cellulose, hemicellulose, fats and starches) are thermally degraded to three different fractions: bio-oil (condensed vapors), char (solid fraction) and non-condensable gases [21]. In general, a higher yield of BC is expected from biomasses that contain more lignin and less cellulose. Also, the porosity of BC increases with the amount of lignin in the biomass [22–24].

Heating rate, residence time and temperature have a direct impact on the distribution and yield of each of these fractions [25,26]. Of these parameters, the maximum temperature to which the biomass is subjected in the pyrolysis reactor, called highest treatment temperature (HTT) has the greatest overall influence on the biochar properties [27–30]. Low-temperature pyrolysis generally produces high BC yields. In contrast, high-temperature pyrolysis leads to BCs with a high C content and large surface area. However, functional groups are likely to be decomposed through heat degradation when higher temperatures are applied [31]. Also, H/C and O/C ratios steadily diminish as the temperature increases, reflecting the loss of easily degradable compounds by dehydration and decarboxylation reactions [32]. This way, it is not easy to deduce which temperature will be most suitable for a biomass' efficient conversion into an adsorbent material bearing the intended specificity.

A large number of feedstock types have been used in the production of BC [33]. Due to their different composition, different biomass yields biochars with different properties [30]. Likewise, different pyrolytic conditions applied to the same biomass have a large effect on biochar's properties, such as surface area and porosity, which are all important parameters affecting biochar's sorption characteristics [34–36].

Macauba (*Acrocomia aculeata*) is a palm tree prevalent in the Brazilian savannah, known as “*cerrado*”. Its fruit is a renewable natural source of vegetable oil for food and cosmetic industries (nut oil) and for biodiesel (mesocarp or pulp oil). The dark stiff nut shell called endocarp, reminiscent of the nut oil extraction, comprises 25% of the fruit mass, has an elevated lignin content (> 30%), and can therefore be exploited as feedstock for biochar production [37].

In this study, the endocarp has been subjected to six different pyrolytic temperatures, aiming to evaluate the effect of the pyrolytic temperature on the biochar derived from the macauba endocarp for the removal of uranium (VI) from aqueous solutions. Proximate analysis was used for the determination of the “proximate” overall composition of the BCs by revealing each BC's unique profile through the assessment of four parameters: moisture, volatile matter, ash content and fixed carbon. The relationship between fixed carbon (FC) and gravimetric yield (GY) allowed the selection of the pyrolytic temperature at which to achieve the most stable material without compromising the yield. In addition, ultimate analysis was performed to assess changes in the elemental composition of BCs produced at different temperatures. However, these parameters, alone, do not suffice in defining which pyrolytic temperature is the most suitable to obtain a BC with the highest adsorption capacity for the removal of uranium from aqueous solutions. Therefore, the effect of the pyrolytic highest treatment temperature (HTT) on the BCs produced at each different temperature was evaluated by adsorption experiments, through which it was possible to obtain the adsorption capacities of the biochars produced at different HTTs. Fourier-transform infrared spectroscopy (FTIR) and X-ray photoelectron spectroscopy (XPS) techniques were used for surface characterization, which helped identify the functional groups involved in the adsorption process.

The removal of uranium using macauba biochar has not been reported in previous studies. This study does not only present the potential of macauba biochar for removing uranium from aqueous solutions, but also highlights the importance of a careful selection of the pyrolytic temperature in order to maximize the adsorbent's removal capacity for uranium and its yield, thus providing a sustainable strategy for the management of both the agro-industry residues and the aqueous wastes containing uranium.

2. Experimental

2.1. Materials

Soleá (João Pinheiro, MG, Brazil) supplied the endocarp from the macauba coconut. The processing involved a depulping step followed by shelling of the chestnut with a jaw crusher, allowing the separation of the endocarp.

A standard solution of 1000 mg L^{-1} of uranium was prepared by dissolution of a U_3O_8 certified reference material (CRM 129-A, natural ^{238}U) supplied by New Brunswick Laboratory (New Brunswick, NJ, USA). Diluted uranium solutions used for calibration and adsorption experiments were prepared with ultrapure water (18.2 MΩ cm resistivity) and Merck's analytical grade nitric acid, HNO_3 65% (Darmstadt, HE, Germany).

All the experiments were conducted with the natural isotope (^{238}U). Considering the number of experiments performed in adsorption studies, limiting the exposure to the radiation is advisable, as well as

minimizing the generation of secondary radioactive waste. Moreover, since isotopes have identical chemical properties, it was possible to simulate the radioactive isotope behavior throughout the entire process using the uranium's natural isotope solution.

2.2. Sample preparation

After sampling for the separation of dirt and unbroken coconuts, the endocarp was ground in a cutting mill passing over a 3/8 Mesh screen for a preliminary homogenization and subsequently oven-dried at 100 °C for 3 h.

2.3. Biochar production

Pyrolysis of the endocarp was carried out using a Thermo Fisher (Asheville, NC, USA), Lindberg Blue M, horizontal tubular steel reactor heated by an electric furnace under inert argon atmosphere. The temperatures used were in the range between 250 °C to 750 °C. The carbonized samples were denominated as "BCT", in which "T" corresponds to the pyrolytic highest treatment temperature, HTT; for instance: "BC450" refers the biochar obtained at 450 °C.

The dried endocarp was subjected to six different HTTs (250 °C, 350 °C, 450 °C, 550 °C, 650 °C and 750 °C) and a heating rate of 5 °C min^{-1} was employed. For each HTT, approximately 30 g of dry endocarp was pyrolysed in argon (Ar) atmosphere (gas flow of 40 mL min^{-1}). The holding time of samples at each HTT was 60 min, followed by natural cooling in the furnace, continuously purged with Ar.

After cooling down to approx. 90 °C, the alumina crucible containing the biochar was removed from the furnace and allowed to cool at room temperature in a desiccator. Finally, the biochar was ground in a cutting mill passing over a 120 Mesh screen and stored in polypropylene flasks from SCP Science (Baie-D'Urfé, QC, Canada).

2.4. Proximate analysis

Proximate analysis was conducted using the standard method ASTM D3172-13 [38]. The gravimetric yield (GY, d.b.) of each recovered biochar was calculated according to Eq. (1).

$$GY(\%) = 100 \times (M_1/M_0) \quad (1)$$

where M_0 is the mass of the oven-dried endocarp, as described in section 2.2, and M_1 is the mass of the biochar after each pyrolysis process.

For moisture content determination (MC, a.r.), about 2 g of each biochar was weighed in a porcelain crucible and oven-dried at 105 °C for 2 h. After cooling at room temperature in a desiccator, the sample was weighted again. The percentage weight loss or MC(%) was calculated as follows:

$$MC(\%) = 100 \times [(M_1 - M_2)/M_1] \quad (2)$$

where M_2 is the mass of the oven-dried biochar.

Volatile matter content (VM, d.b.) was determined subjecting the biochar obtained in the moisture test to a temperature of 950 °C for 11 min. VM is calculated according to Eq. (3).

$$VM(\%) = 100 \times [(M_2 - M_3)/M_2] \quad (3)$$

where M_3 is the mass of the biochar after devolatilization at 950 °C.

Ash content (AC, d.b.) was determined using the biochar previously calcined for the volatile matter content test, for which, approximately 1 g of the calcination residue was subjected to combustion in an uncovered crucible at 750 °C for a minimum of 2 h. The resulting mass was weighted after the material was allowed to cool at room temperature in a desiccator and the ash content was calculated according to Eq. (4).

$$AC(\%) = 100 \times (M_4/M_2) \quad (4)$$

where M_4 is the residual ash mass.

The fixed carbon content (FC, d.b.) was determined according to the following equation:

$$FC(\%) = 100 - [VM(\%) + AC(\%)] \quad (5)$$

Finally, the gravimetric yield factor (GYF) is defined as the product of fixed carbon content and the gravimetric yield and was calculated as it follows:

$$GYF(\%) = GY(\%) \times FC(\%) \quad (6)$$

2.5. Ultimate analysis

Ultimate analysis (C, H, O, N, S) was performed using two elemental LECO analyzers, TCHEN600 and CS-400 (Saint Joseph, MI, USA), the first for H, O and N detection and the second for C and S detection.

2.6. Adsorption experiments

Equilibrium adsorption experiments were conducted using batch technique and the experiments were performed in a rotary shaker using 100 mL glass beakers, 120 rpm stirring rate at room temperature (25 °C) during 24 h. The adsorbent was separated by filtration using a 0.45 micron Teflon membrane SCP Science filter (Baie-D'Urfé, QC, Canada).

The U(VI) concentration in the remaining filtrate solution was subjected to quantification by inductively coupled plasma optical emission spectrometry using a Spectro ARCOS ICP OES (Kleve, NRW, Germany).

The adsorption capacity, q_t (mg g^{-1}), of the adsorbent was calculated using Eq. (7):

$$q_t = [(C_0 - C_t) \times V]/M \quad (7)$$

where q_t is the adsorbed amount of adsorbate per gram of adsorbent at any time t, C_0 and C_t the concentrations of the adsorbate in the initial solution and at any time t, respectively (mg L^{-1}); V the volume of the adsorbate solution added (L) and M the amount of the adsorbent used (g).

The extraction efficiency, R (%), was determined through the following equation:

$$R(\%) = 100 \times [(C_0 - C_t)/C_0] \quad (8)$$

where R is the efficiency of extraction or retention percentage, C_0 (mg L^{-1}) is the initial concentration of each adsorbate and C_t (mg L^{-1}) represents the concentration of the adsorbate at time t.

2.7. Surface characterization

Surface analysis was carried out using a PerkinElmer Spectrum One FTIR spectrophotometer (Waltham, MA, USA) and a Thermo K-Alpha X-ray photoelectron spectrometer (Asheville, NC, USA).

3. Results and discussion

3.1. Proximate analysis

The results of the proximate analysis of the biochars obtained in different HTTs are shown in Table 1.

As the pyrolysis temperature was increased, the gravimetric yield decreased with progressing thermal decomposition of the constituents of the endocarp. At the same time, fixed carbon content increased with increasing HTT, while volatile matter content decreased.

Ash content is a measure of the total amount of minerals remaining after the water and the organic matter have been removed by heating. As noted in Table 1, the AC of the resulting biochars increased with increasing temperatures. The increase in AC is the result of the

Table 1
Proximate analysis of the macauba biochars.

Parameter	GY(%)	MC(%)	VM(%)	AC(%)	FC(%)
BC250	75.21	2.20	67.84	2.31	29.85
BC350	46.09	1.57	36.70	3.08	60.22
BC450	38.88	1.46	28.81	2.40	68.78
BC550	35.57	1.31	20.23	2.42	77.35
BC650	34.10	1.22	16.78	3.21	80.01
BC750	33.44	1.01	14.01	3.87	82.13

*GY = gravimetric yield; MC = moisture content; VM = volatile matter; AC = ash content; FC = fixed carbon.

Table 2
Elemental analysis of the macauba endocarp and the biochar according to the pyrolytic temperatures.

Parameter	C(%)	H(%)	O(%)	N(%)	S(%)	H/C	O/C	(O + N)/C
Endocarp	50.6	6.37	47.4	1.02	0.32	0.130	0.940	0.960
BC250	52.4	2.85	44.6	0.75	0.26	0.054	0.851	0.865
BC350	57.5	2.18	28.1	0.59	0.25	0.038	0.489	0.499
BC450	62.4	2.14	23.2	0.57	0.24	0.034	0.372	0.381
BC550	69.5	2.13	22.4	0.53	0.24	0.031	0.322	0.330
BC650	70.8	1.69	17.8	0.51	0.23	0.024	0.251	0.259
BC750	75.1	1.56	16.5	0.41	0.23	0.021	0.220	0.225

*C = carbon; H = hydrogen; O = oxygen; N = nitrogen; S = sulfur; H/C = hydrogen:carbon ratio; O/C = oxygen:carbon ratio; (O + N)/C = oxygen and nitrogen:carbon ratio.

progressive concentration of minerals and destructive volatilization of the lingo-cellulosic structure as temperature increased [39,40]. Comparable findings in the literature describe an exponential increase of AC with the pyrolytic temperature [41–45]. The variation in the results can be ascribed to sample inhomogeneity.

A significant increase in fixed carbon was observed between 250 and 350 °C, mainly due to the loss of the volatile matter. This way, O and H were initially lost in the form of water and, further in the form of light hydrocarbons, carbon monoxide and carbon dioxide, as shown in Table 2. As a result, carbon gets concentrated in the material as the HTT rises. Fixed carbon content tended to stabilize at higher temperatures (higher than 550 °C). As shown in Table 1, there was little variation in the fixed carbon content among 550, 650 and 750 °C.

The gravimetric yield factor (GYF) was required to identify the temperature at which to obtain a biochar with the maximum fixed carbon content and gravimetric yield [46]. The GYF as a function of the pyrolytic temperature is shown in Fig. 1.

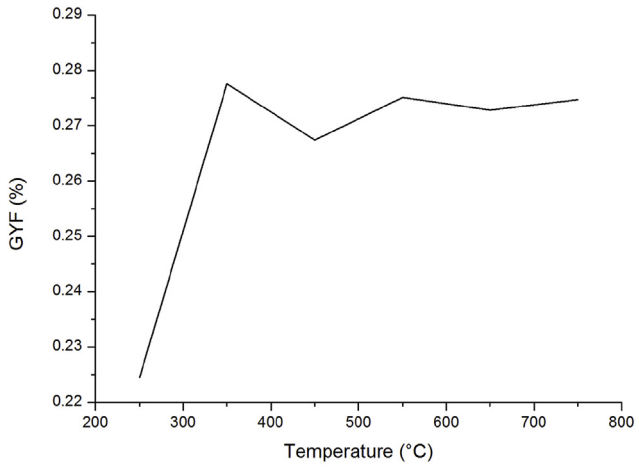

Fig. 1. Gravimetric yield factor (GYF) as a function of the pyrolytic temperature.

The GYF obtained for BC350 was 0.28%, whereas the one for BC250 was 0.22%. For temperatures higher than 350 °C, the factor levelled off around 0.27% and remained nearly constant, with no significant variability (± 0.002% fluctuation), indicating that any possible gravimetric gain wouldn't justify the time and energy requirements of working at higher temperatures. Based on this measure, the production of biochar at temperatures higher than 350 °C would be unnecessary. Similar stabilization trend in yield of fixed carbon at temperatures above 350 °C has been shown for other types of biomass as well [47] and is therefore not specific to macauba endocarp.

Notably, pyrolytic temperature is a defining parameter on the biochar's properties, such as the availability of surface functional groups and porosity [30]. Therefore, GYF alone cannot be used to designate the temperature at which to produce a good adsorbent [48–53]. Adsorption experiments are necessary to evaluate the temperature to which the macauba endocarp should be subjected in order to produce a biochar with the highest adsorption capacity for U(VI).

3.2. Elemental analysis

The results of the elemental analysis of the macauba endocarp and the biochars obtained at different temperatures are shown in Table 2.

These results are in accordance with other studies, which demonstrated that the carbon content increases with the increase of the pyrolytic temperature [54–58], while the nitrogen content is only minimally affected by the pyrolytic temperature [59,60] and depends mainly on biomass feedstock.

It can be seen in Table 2 that the carbon content increased with the pyrolytic temperature, whereas the decrease of the oxygen and hydrogen contents resulted in the decrease of the H/C, O/C and (O + N)/C molar fractions.

Fraction H/C is typically used to describe the degree of carbonization, since H is mainly associated with the organic matter of the biomass. Carbon content is commonly used to qualify chars that are going to be used as fuel sources, but may also be responsible for the adsorption properties of chars. The extent of charring is also related to the progression of deoxygenation, which can be described by the O/C fraction. The O/C ratios assigned to materials shows a systematic increase from 0 for graphite to > 0.6 for materials not considered to be black C [61].

Adsorbent materials benefit from higher O and H containing groups, which provide binding sites to target substances. The hydrophilicity of the biochar's surface can be inferred from the O/C molar fraction, because O content is indicative of the presence of polar groups [62,63]. Thus, a decrease in the O/C fraction indicates that the surface of the biochar is more aromatic and less hydrophilic. This is due to the greater extent of carbonization and the loss of polar functional groups at elevated temperatures [64–66], as shown at the Van Krevelen graph in Fig. 2. The decrease in the (O + N)/C fraction also reflects the decrease of polar groups as the pyrolytic temperature is increased [57,67].

The correlation between H/C ratio and fixed carbon content (Fig. 3) indicated that fixed carbon has a very low H content and also that volatile matter released during pyrolysis consisted of compounds with higher H/C ratios than the remaining biochar. Hence, the devolatilization removed most of the H from the biomass as the pyrolysis conversion reaction took place.

3.3. Adsorption on different BCs

The adsorption capacity of the BCs obtained in different pyrolytic temperatures were evaluated for a 5 mg L^{-1} U(VI) solution adjusted to pH 3, using an adsorbent dose of 10 g L^{-1}. These adsorption parameters have been previously established through experimentation and optimized for maximum uranium removal [68]. The results for each obtained BC are shown in Table 3.

The relationship between the pyrolytic temperature at which each

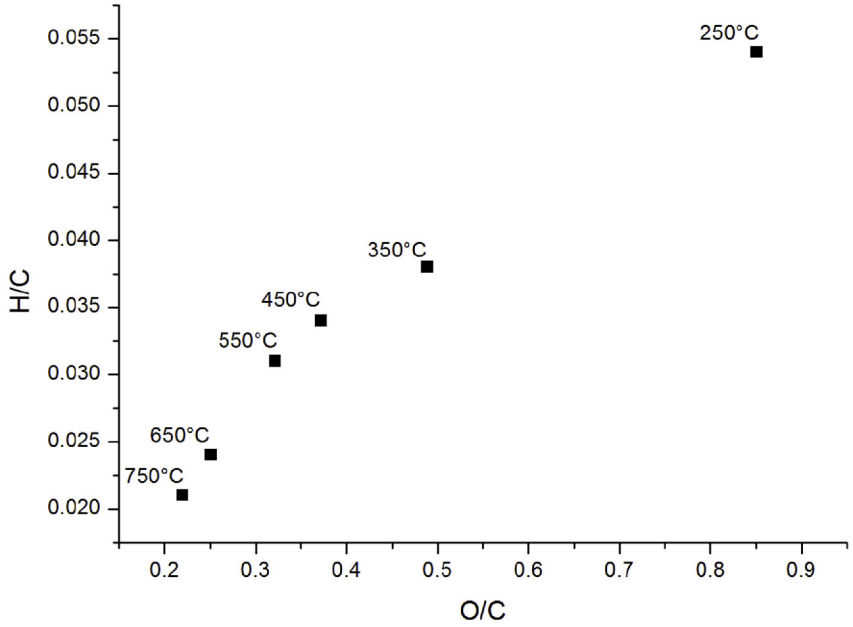

Fig. 2. Van Krevelen graph for the elemental fractions of the biochar obtained from the macauba endocarp at different pyrolytic temperatures.

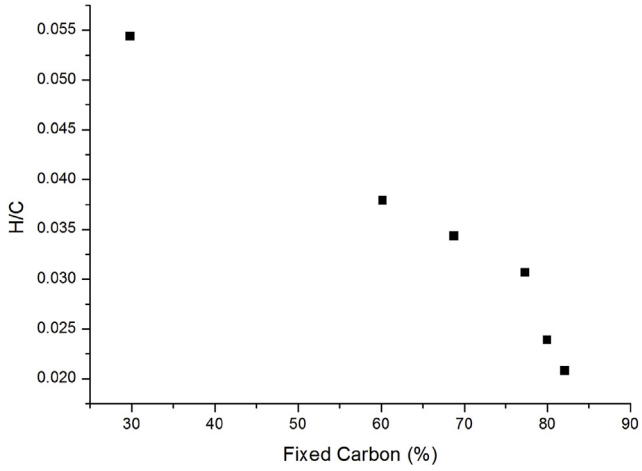

Fig. 3. H/C ratio versus fixed carbon (FC) content.

Table 3
The influence of pyrolytic temperature on the removal of U ions.

BC	qt (mg g^{-1})	R (%)
250	417	85.9
350	408	80.1
450	372	75.8
550	88	17.7
650	56	10.9
750	52	10.4

BC was obtained with the adsorption capacity is illustrated in Fig. 4. Removal above 75% was achieved for temperatures under 450 °C, and the highest adsorption capacity was achieved at 250 °C. A drastic decrease of the adsorption capacity was observed when the endocarp was subjected to temperatures higher than 450 °C, suggesting that the presence of oxygenated functional groups is crucial to the adsorption of uranyl ions onto the biochar's surface.

According to Fig. 4, BC250 should be preferably selected over BC350 for treatment of uranium from aqueous solutions, because of its high adsorption capacity. However, the gain in adsorption doesn't justify the loss in fixed carbon content (only 6% points more removal efficiency at the expense of 33.47% points of fixed carbon content). Also, as shown by the proximate analysis, at 350 °C, it was possible to achieve a BC with a higher fixed carbon content without severely compromising the gravimetric yield. Fixed carbon content is a good measure of stability [46], a desired quality for a material that will be used as substrate for radioactive uranium and, therefore, will require long-term storage. Although it is possible to obtain even higher fixed carbon contents by increasing the pyrolytic temperature, this quality is secondary compared to the adsorption capacity required for a more efficient removal and, consequently, a more effective treatment of the targeted solution. Therefore, a compromise between efficiency and stability should be met.

Also, according to CNEN's regulation CNEN-NN-8.01 [9], if either BC250 or BC350 should be selected to treat uranium-containing aqueous wastes with an initial concentration of 5 mg L^{-1}, none of the BCs would meet the allowable limits for discharge. When BC250 was used as adsorbent, the remaining U concentration was of approx. 0.705 mg L^{-1} (705 ppb). For BC350, the remaining U concentration was of approx. 0.995 mg L^{-1} (995 ppb). CNEN's allowable limits depend on the isotopic mixture and can be a minimum of 0.070 mg L^{-1} (70 ppb) for 100% U-235 and a maximum of 0.450 mg L^{-1} (450 ppb) for natural uranium (approx. 100% U-238). Brazil is strongly committed to the Treaty on the Non-Proliferation of Nuclear Weapons (1970), being only allowed to use uranium enriched to less than 20% U-235 (*low-enriched uranium* or LEU). For approx. 20% U-235, which would be the maximum allowable enrichment degree, the allowable limits according to CNEN's regulation would be of 0.217 mg L^{-1} (217 ppb), approx. 3.2 times less the concentration achieved when BC250 was used and 4.5 times less the concentration achieved when BC350 was used.

Although neither BC250 nor BC350 would meet the required limits for a safe release of the treated water, they considerably decrease the concentration of uranium in the solution, and could have a practical application in a multi-stage separation, in which any remaining U would be removed in a polishing stage using another sorbent. Due to the fact that the most effective biochar for U removal was produced from a low-value residue and at mild processing conditions (low pyrolysis temperature), such material would be cheap, while offering good adsorption capacity, leaving only small amounts of U to be removed in

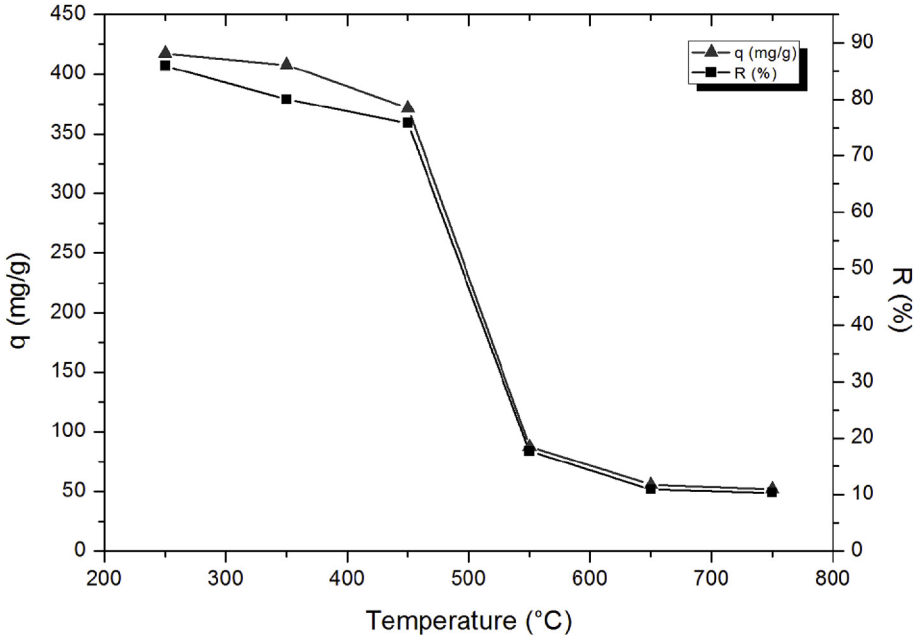

Fig. 4. Effect of the pyrolytic temperature on the adsorption of U(VI) onto BCs produced at different temperatures; *pH* = 3; *adsorbent dose* = 10 g L^{-1}; initial *concentration* = 5 mg L^{-1}; *contact time* = 24 h; *temperature* = 25 ± 2 °C.

the next stage of separation process by other, potentially more expensive materials. Therefore, such approach would offer considerable economic and environmental benefits.

3.4. Surface characterization

3.4.1. FTIR analysis

The superposition of the FT-IR spectra for the BCs obtained for each pyrolytic temperature tested is presented in Fig. 5. The results showed that the pyrolytic temperature had a considerable influence upon the surface functional groups of the macauba biochar.

Lignocellulosic materials are polymers rich in hydroxide groups. After pyrolysis, the peak at 3400 cm^{-1}, which can be assigned to –OH stretching, got significantly lower as the temperature increased and even disappeared at higher temperatures (> 550°). Aliphatic stretches C – H were observed at 2940 cm^{-1}, showing that the cellulose was not entirely carbonized at lower temperatures (< 350 °C), but got fully degraded as the temperature rose. The stretching band at 1270 cm^{-1},

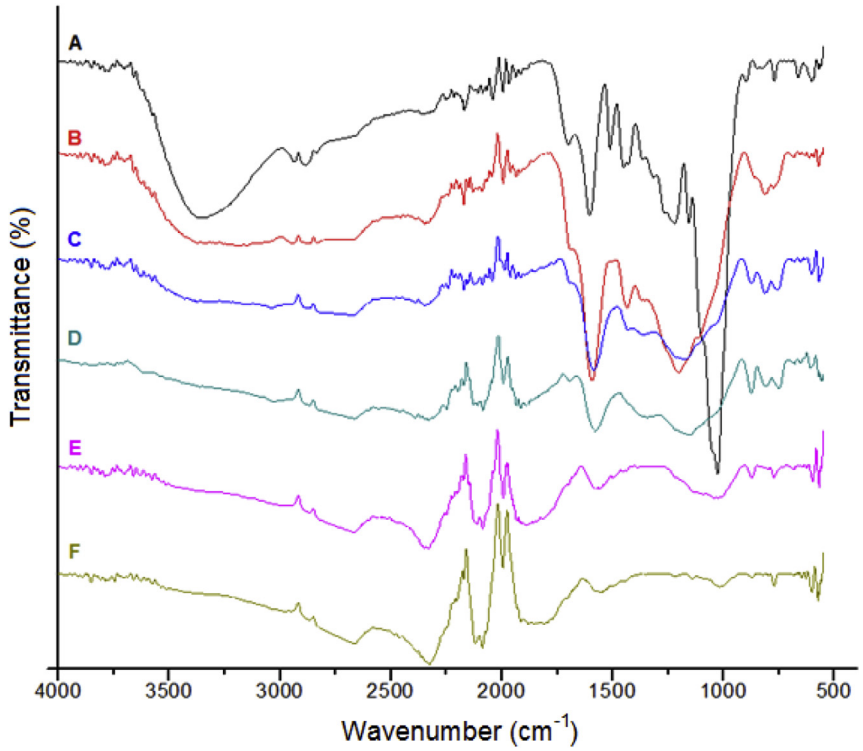

Fig. 5. Superposition of FT-IR/UATR spectra of the macauba biochars produced at different pyrolytic temperatures: 250 °C (A), 350 °C (B), 450 °C (C), 550 °C (D), 650 °C (E), 750 °C (F).

corresponding to the aromatic –CO and the phenolic –OH, also decreased with temperature due to the increase of the pyrolysis reaction of the different constituents of the macauba endocarp [69].

A broad unsymmetrical peak with a maximum at 1744 cm^{-1} could be attributed to C=O stretching. This peak comprises a variety of C=O containing functional groups, including ketones, carboxylic acids esters, lactones and anhydrides. The band at 1605 cm^{-1} could be assigned to C=C bond stretching derived from aromatic rings in the lignin, as well as newly aromatized and carbonized material from carbohydrate ring dehydration and cyclisation during pyrolysis [70]. Both these bands, at 1744 and 1605 cm^{-1}, have initially increased and further decreased with the increase of the temperature, in agreement with the literature [71].

Peaks expected from single bond stretching and other deformation bands in the region 1500 to 650 cm^{-1} were also observed. Since these were numerous and overlapped, it was difficult to assign each of them in the spectrum.

These spectra are in agreement with the changes in the elemental composition and with the process of decomposition of crude biomass, indicating that the increase of the pyrolytic temperature causes the decrease of the acidity and the polarity in the surface of the produced biochar, at the same time that it increases the aromaticity of it [54,59,71].

These findings corroborate the fact that the surface functional groups play an important role in the U(VI) adsorption. The adsorption of U(VI) was notably higher on BCs produced at lower temperatures, indicating a dependency on the polar organic sites in the adsorbent. In this case, chemisorption is the main adsorption mechanism, since UO_2^{2+} can make bonds with carboxyl, carbonyl and hydroxyl groups.

The overlap of the infrared transmission spectra using diffuse reflectance (DRIFT) mode of the BC350 alone (A) and the BC350 loaded with U (B) is presented in Fig. 6. The differences in stretching can be attributed to changes in the vibrational modes resulting from the association with the uranyl ion after the adsorption. These differences are very subtle due to the low uranium concentration employed in the tests.

After adsorption of U(VI), the peaks at 3400, 1608, 1442 and 841 cm^{-1} were displaced to 3478, 1627, 1456 and 861 cm^{-1} respectively. This shift to lower energy, called “redshift”, occurs because the uranium “weighs” at the vibration of the chemical group, being shifted to a lower energy. The peak at 2938 cm^{-1} is decreased and the peak at 1237 cm^{-1} is practically absent after adsorption of U(VI).

These results indicate that the groups O–H (3600-3200 cm^{-1}, corresponding to the alcohol O–H stretch and 3400-2500 cm^{-1}, corresponding to the carboxylic acid O–H stretch), C=C (1680-1600 cm^{-1}, corresponding to C=C of alkenes and 1600-1400 cm^{-1}, corresponding to C=C of aromatic structures) and C–O (1320-1210 cm^{-1}, corresponding to acyl groups in carboxylic acids and 1260-1000 cm^{-1}, corresponding to the alcoxy groups in alcohols) can bind to the uranyl cations (UO_2^{2+}).

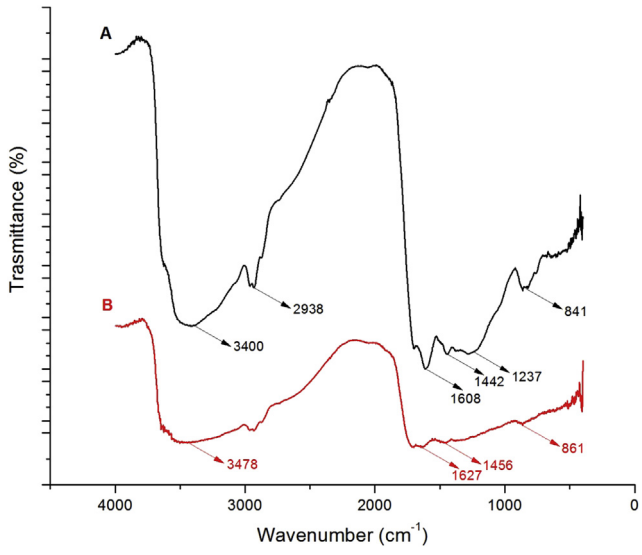

Fig. 6. Comparison of the FTIR/DRIFT spectra of the BC350 (A) and BC350 after the U(VI) adsorption (B).

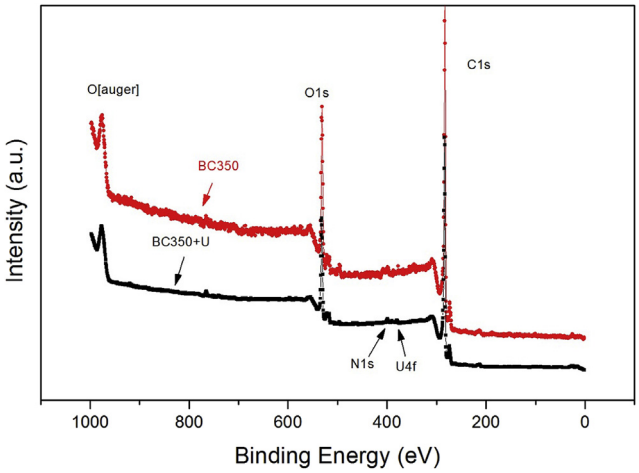

Fig. 7. XPS spectra of BC350 before and after adsorption of U (VI).

In fact, the O atom ($1s^2 2s^2 2p_x^2 2p_y^1 2p_z^1$) on hydroxyl groups adopts a sp^3 type of hybridization to form four sp^3 orbitals, which can promote bonds with H atoms. In addition, the two remaining sp^3 orbitals can be occupied by two solitary pairs of electrons for the O atom. These solitary pairs of electrons can bind with the positively charged uranyl ions, thereby promoting the occurrence of the chemisorption [72].

3.4.2. XPS analysis

X-ray photoelectron spectroscopy (XPS) was employed to provide the elemental composition and a first insight into the bonding environment of the U adsorbed onto the BC350's surface. As seen in Fig. 7, the BC350 spectrum consisted of peaks corresponding to the atoms of carbon (C 1s), oxygen (O 1s) and nitrogen (N 1s). A new peak emerged in the XPS spectrum of the BC350 loaded with U (BC350 + U) next to the peak K 2s in 377.63 eV.

In order to better resolve the peaks for each of the atoms present, the spectra in Fig. 7 were deconvoluted and analyzed using the XPSPEAK 41 Gaussian Adjustment Software. Deconvolution of the C 1s spectrum before and after the adsorption of U(VI) can be visualized in Figs. 8 and 9, respectively.

Three peaks were observed in the XPS C 1s spectrum of BC350 (Fig. 8), including C–C (284.8 eV), C–O (286.5 eV) and C=O (288.4 eV). An interpretation of the most usual peaks in the XPS C 1s spectrum is presented in Table 4.

The XPS spectrum in Fig. 9 shows the deconvolution of the C1s peak of the BC350 after the U (VI) adsorption. Two peaks remain, with binding energies at 284.6 eV and 287.5 eV, attributed to the C–C bonds of aromatic and aliphatic chains and C=O bonds of carbonyl groups, respectively. The peak at 286.5 eV, related to the C–O bond of hydroxyl and carboxylic acid groups disappeared after adsorption of U by BC350, corroborating the FTIR results.

The peak of U4f, originally present in the spectrum of BC350 after the U (VI) adsorption, could be converted into two intense peaks between 375 and 410 eV, one with a binding energy centered between 381 and 382 eV and the other located between 391 and 392 eV (Fig. 10).

According to the NIST database [73], the peaks at 381.3 and 391.5 eV can be attributed to the U “f” orbitals $4f_{7/2}$ and U $4f_{5/2}$ of uranyl nitrate, $UO_2(NO_3)_2$ [74–76].

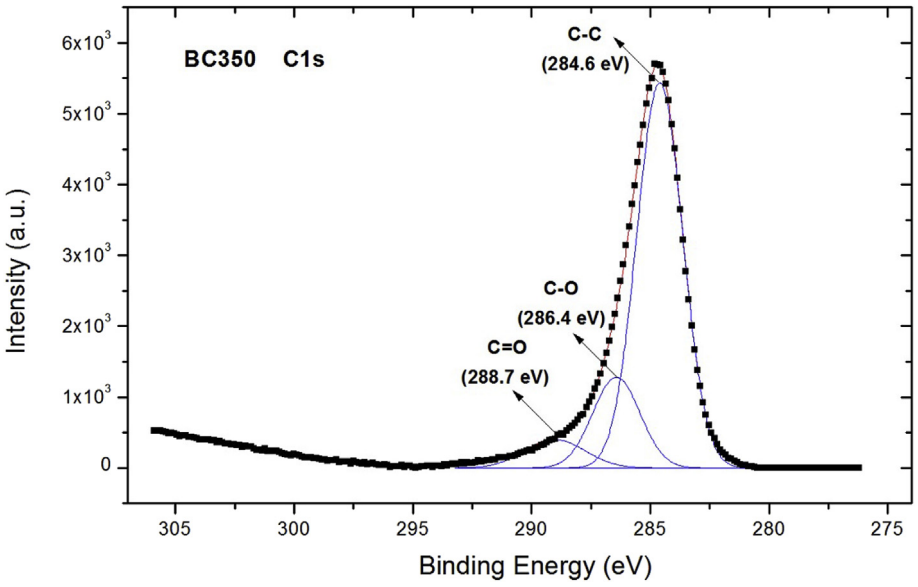

Fig. 8. Deconvolution of the XPS C1s peak before adsorption of U (VI) onto BC350.

XPS analysis was able to detect the U after adsorption, thereby, confirming that the U was actually adsorbed onto the BC350. In addition, XPS analysis reaffirmed the results obtained by FTIR, showing that chemisorption has been in fact enabled by oxygenated groups (hydroxyl and carboxylic acid groups) of the BC350's functionalized surface.

4. Conclusion

The results of this study indicate that macauba biochar's properties and stability are greatly influenced by the pyrolytic temperature. Biochar yield and volatile matter decreased with the increase of the pyrolytic temperature, whereas the fixed carbon content increased with increasing temperatures. The gravimetric yield factor provided the best compromise between fixed carbon content and gravimetric yield, which was achieved for the biochar obtained at 350 °C. As pyrolysis progressed, hydrogen, oxygen, nitrogen and sulfur were preferentially released in form of volatiles and gases. FTIR analysis evidenced that the biochars obtained at lower temperatures present more polar organic sites, promoting the adsorption of U (VI) by chemisorption. XPS analysis indicated that hydroxyl and carboxylic acid groups were involved in binding the uranyl ions onto the biochar's surface. A removal efficiency of 80% was achieved for the biochar produced at 350 °C, demonstrating its potential as value-added material for U (VI) removal from aqueous solutions in multi-stage systems. Future studies should be directed towards a better understanding of the characteristics of the

Table 4
Allocation of peaks in the XPS spectrum of C 1s.

Binding energy (eV)	Assignment
285.0	Aromatic and aliphatic structures. Binding of C atoms with H and C atoms
286.0	Simple C-O bond (alcohol, ether, carboxylic acid)
287.5	C=O double bond (carbonyl)
289.0	O-C = O (carboxylic acid, ester)
290.5	Carbonate, CO_2
291.5	Plasmon

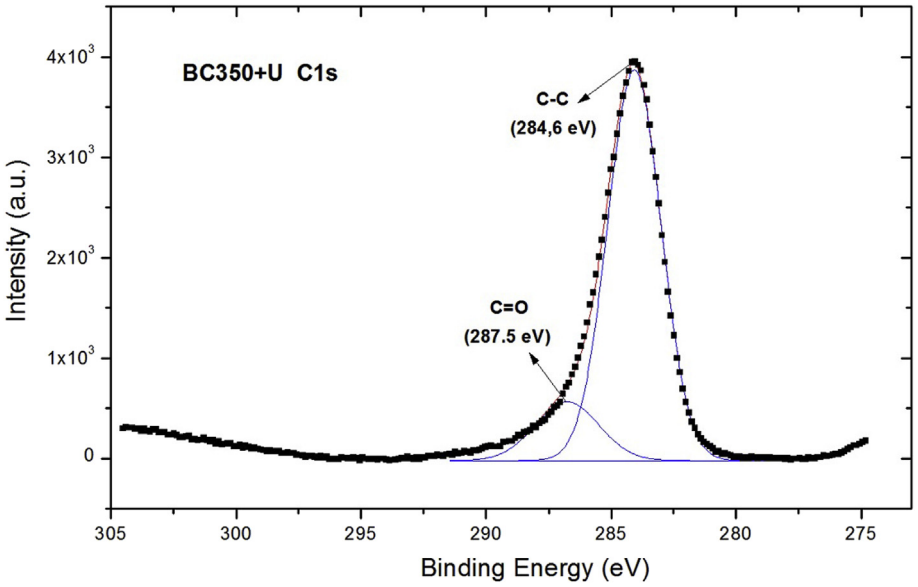

Fig. 9. Deconvolution of the XPS C1s peak after adsorption of U (VI) onto BC350.

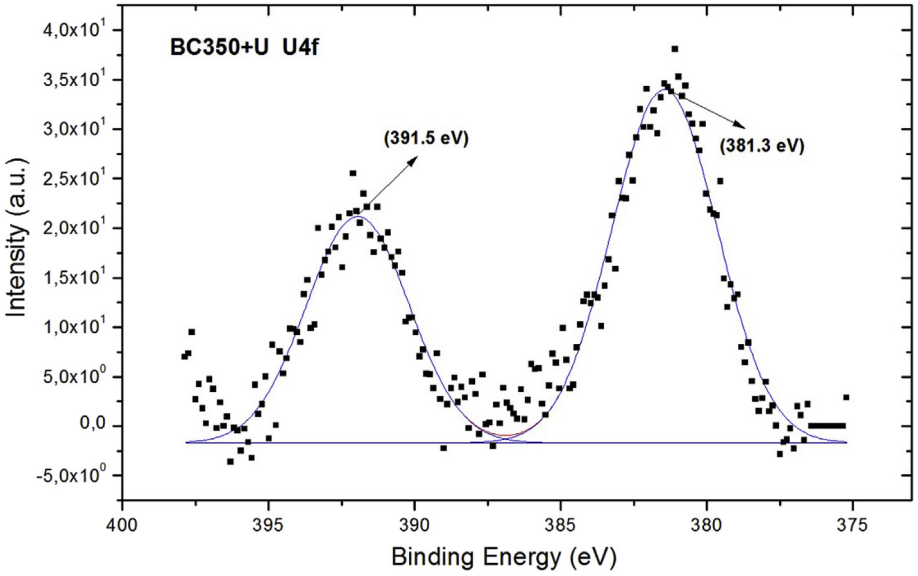

Fig. 10. Deconvolution of the peak U4f after adsorption of U (VI) onto BC350.

macauba biochar that influence the U (VI) removal from aqueous solutions. Also, macauba biochar may be tested for the treatment of other radioactive contaminants.

Acknowledgements

The authors would like to thank Dr. Jorge Alberto Soares Tenório from the Waste and Metallurgy Recycling Laboratory (LAREX, Poli/USP-SP) and his PhD student, Jorge Coleti, for the support in the pyrolysis process. We are also immensely grateful to Mr. Felipe Morbi from Soleá Brasil (João Pinheiro, Brazil) for supplying the macauba endocarp.

References

[1] IAEA, Standardization of Radioactive Waste Categories, International Atomic Energy Agency, Vienna, 1970 (IAEA-TECDOC-101).
[2] IAEA, Predisposal Management of Radioactive Waste (IAEA Safety Standards Series No. GSR Part 5), International Atomic Energy Agency, Vienna, 2009.
[3] OECD, Radioactive Waste in Perspective (NEA No. 6350), Organization for Economic Co-Operation and Development, Paris, 2010.
[4] M. Linardi, O IPEN e a Inovação Tecnológica, SENAI-SP editora, São Paulo, 2016 [Portuguese].
[5] USDHHS, Toxicological Profile for Uranium, Agency for Toxic Substances and Disease Registry (ASTDR), United States Department of Health and Human Services, Atlanta, 2013.
[6] S.R. Jorgensen, B. Fath, Encyclopedia of Ecology, Elsevier B. V., Amsterdam, 2008.
[7] IAEA, Combined Methods for Liquid Radioactive Waste Treatment, International Atomic Energy Agency, Vienna, 2003 (IAEA-TECDOC-1336).
[8] IAEA, Management of Discharge of Low Level Liquid Radioactive Waste Generated in Medical, Research and Industrial Facilities, International Atomic Energy Agency, Vienna, 2013 (IAEA-TECDOC-1714).
[9] CNEN, Gerência de rejeitos radioativos de baixo de médio níveis de radiação (CNEN-NN-8.01), Comissão Nacional de Energia Nuclear, Rio de Janeiro, 2014 [Portuguese].
[10] H.E.-D.M. Saleh, T. Bayoumi, S. Eskander, Characterizations of polyester cement composites used for the immobilization of radioactive wastes, in: H.E.-D.M. Saleh (Ed.), Polyester, InTech Open Access, London, 2012.
[11] R. V. de P. Ferreira, Aplicação de biossorventes no tratamento de rejeitos radioativos líquidos [thesis], Instituto de Pesquisas Energéticas e Nucleares, São Paulo, 2014 [Portuguese].
[12] CNEN, Critérios de aceitação para deposição de rejeitos radioativos de baixo e médio níveis de radiação (CNEN-NN-6.09), Comissão Nacional de Energia Nuclear, Rio de Janeiro, 2002 [Portuguese].
[13] S. De Gisi, G. Lofrano, M. Grassi, M. Notarnicola, Characteristics and adsorption capacities of low-cost sorbents for wastewater treatment: a review, Sustain. Mater. Technol. 9 (2016) 10–40.
[14] M. Keiluweit, M. Kleber, Molecular-level interactions in soils and sediments: the role of aromatic pi-systems, Environ. Sci. Technol. 43 (10) (2009) 3421–3429.
[15] J.L. Field, C.M.H. Keske, G.L. Birch, M.W. Defoort, M.F. Cotrufo, Distributed biochar and bioenergy coproduction: a regionally specific case study of environmental benefits and economic impacts, GCB Bioenergy 5 (2) (2013) 177–191 2013.
[16] D. Kołodynska, R. Wnetrzak, J. Leahy, M. Hayes, W. Kwapinski, Z. Hubicki, Kinetic and adsorptive characterization of biochar in metal ions removal, Chem. Eng. J. 197 (2012) 295–305.
[17] M.I. Inyang, B. Gao, Y. Yao, Y. Xue, A. Zimmerman, A. Mosa, P. Pullammanappallil, Y.S. Ok, X. Cao, A review of biochar as a low-cost adsorbent for aqueous heavy metal removal, Crit. Rev. Environ. Sci. Technol. 46 (4) (2016) 406–433.
[18] J.M. Patra, S.S. Panda, N.K. Dhal, Biochar as a low-cost adsorbent for heavy metal removal: a review, Int. J. Res. Biosci. 6 (1) (2017) 1–7.
[19] S.J. Lehmann, Biochar for Environmental Management, Earthscan, Oxford, 2009.
[20] H.M. Freeman, E.F. Harris, Hazardous Waste Remediation: Innovative Treatment Technologies, Technomic Publishing Co. Inc., Lancaster, 1995.
[21] D. Mohan, C.U. Pittman, P.H. Steele, Pyrolysis of wood/biomass for bio-oil: a critical review, Energy Fuels 20 (2006) 848–889.
[22] L. Yang, M. Jin, C. Tong, S. Xie, Study of dynamic sorption and desorption of polycyclic aromatic hydrocarbons in silty-clay soil, J. Hazard Mater. 244–245 (2013) 77–85.
[23] V.J. Bruckman, E.A. Varol, B.B. Uzun, J. Liu, Biochar: A Regional Supply Chain Approach in View of Climate Change Mitigation, Cambridge University Press, Cambridge, 2016.
[24] A. Shariff, N.S.M. Aziz, N. Md. Saleh, N.S.I. Ruzali, The effect of feedstock type and slow pyrolysis temperature on biochar yield from coconut wastes, Int. J. Chem. Mol. Nucl. Mat. Metallurg. Eng. 10 (2016) 1335–1339.
[25] A.V. Bridgwater, G.V.C. Peacocke, Fast pyrolysis processes for biomass, Renew. Sustain. Energy Rev. 4 (2000) 1–73.
[26] Q. Lu, W.-Z. Li, X.-F. Zhu, Overview of fuel properties of biomass fast pyrolysis oils, Energy Convers. Manag. 50 (2009) 1376–1383.
[27] M.J.J. Antal, M. Gronli, The art, science, and technology of charcoal production, Ind. Eng. Chem. Res. 42 (2003) 1619–1640.
[28] A.C. Lua, T. Yang, J. Guo, Effects of pyrolysis conditions on the properties of activated carbons prepared from pistachio-nut shells, J. Anal. Appl. Pyrol. 72 (2004) 279–287.
[29] D. Özçimen, A. Ersoy-Meriçboyu, A study on the carbonisation of grapeseed and chestnut shell, Fuel Process. Technol. 89 (2008) 1041–1046.
[30] L. Zhao, X. Cao, O. Masek, A. Zimmerman, Heterogeneity of biochar properties as a function of feedstock sources and production temperatures, J. Hazard Mater. 256–257 (2013) 1–9.
[31] K. Jindo, H. Mizumoto, Y. Sawada, M.A. Sanchez-Monedero, T. Sonoki, Physical and chemical characterization of biochars derived from different agricultural residues, Biogeosciences 11 (2014).
[32] K.A. Spokas, Review of the stability of biochar in soils: predictability of O:C molar ratios, Carbon Manag. 1 (2010) 289–303.
[33] D. Angin, Effect of pyrolysis temperature and heating rate on biochar obtained from pyrolysis of safflower seed press cake, Bioresour. Technol. 128 (2013) 593–597 2013.
[34] M. Keiluweit, P.S. Nico, M.G. Johnson, M. Kleber, Dynamic molecular structure of plant biomass–derived black carbon (biochar), Environ. Sci. Technol. 44 (2010) 1247–1253.
[35] S.P. Sohi, E. Krull, E. Lopez-Capel, R. Bol, A review of biochar and its use and function in soil, Adv. Agron. 105 (2010) 47–82.
[36] K. Sun, K. Ro, M.X. Guo, J. Novak, H. Mashayekhi, B. Xing, Sorption of bisphenol A, 17a–ethinyl estradiol and phenanthrene on thermally and hydrothermally produced biochars, Bioresour. Technol. 102 (2011) 5757–5763.
[37] R.D.F. Rios, R.M. Fonseca, E.C. Cren, M.H.C. Andrade, Adsorção de fenol no carvão ativado produzido a partir do endocarpo do fruto da macaúba, Proceedings of the

XX Congresso Brasileiro de Engenharia Química, COBEQ 2014, Oct 19-22, Florianópolis, 2014 [Portuguese].
[38] ASTM, Standard Practice for Proximate Analysis of Coal and Coke, American Society for Testing and Materials, Pennsylvania, 2013 (ASTM D3172-13).
[39] X. Cao, W. Harris, Properties of dairy-manure-derived biochar pertinent to its potential use in remediation, Bioresour. Technol. 101 (14) (2010) 5222–5228.
[40] W.T. Tsai, S.C. Liu, H.R. Chen, Y.M. Chang, Y.L. Tsai, Textural and chemical properties of swine-manure derived biochar pertinent to its potential use as a soil amendment, Chemosphere 89 (2) (2012) 198–203.
[41] A. Enders, K. Hanley, T. Whitman, S. Joseph, J. Lehmann, Characterization of biochars to evaluate recalcitrance and agronomic performance, Bioresour. Technol. 114 (2012) 644–653.
[42] J.A. Capunitan, S.C. Capareda, Assessing the potential for biofuel production of corn stover pyrolysis using a pressurized batch reactor, Fuel 95 (2012) 563–572.
[43] S.C. Peterson, M.A. Jackson, Simplifying pyrolysis: using gasification to produce corn stover and wheat straw biochar for sorptive and horticultural media, Ind. Crop. Prod. 53 (2014) 228–235.
[44] A.B. Fuertes, M.C. Arbestain, M. Sevilla, J.A. MacIá-Agulló, S. Fiol, R. López, R.J. Smernik, W.P. Aitkenhead, F. Arce, F. Macias, Chemical and structural properties of carbonaceous products obtained by pyrolysis and hydrothermal carbonisation of corn stover, Aust. J. Soil Res. 48 (6–7) (2010) 618–626.
[45] C.A. Mullen, A.A. Boateng, N.M. Goldberg, I.M. Lima, D.A. Laird, K.B. Hicks, Bio-oil and bio-char production from corn cobs and stover by fast pyrolysis, Biomass Bioenergy 34 (1) (2010) 67–74.
[46] A.L. da Róz, J.F.C. Ricardo, G.T. Nakashima, L.R.O. Santos, F.M. Yamaji, Maximização do teor de carbono fixo em biocarvão aplicado ao sequestro de carbono, Rev. Bras. Eng. Agrícola Ambient. 19 (8) (2015) 810–814 [Portuguese].
[47] O. Masek, P. Brownsort, A. Cross, S. Sohi, Influence of production condutions on the yield and environmental stability of biochar, Fuel 103 (2013) 151–155.
[48] P. Khare, D.K. Goyal, Effect of high and low rank char on soil quality and carbon sequestration, Ecol. Eng. 52 (2013) 161–166.
[49] H. Lu, W. Zhang, Y. Yang, X. Huang, S. WANG, R. Qiu, Relative distribution of Pb^{2+} sorption mechanisms by sludge derived biochar, Water Res. 46 (3) (2012) 854–862.
[50] J. Sun, F. Lian, Z. Liu, L. Zhu, Z. Song, Biochars derived from various crop straws: characterization and Cd (II) removal potential, Ecotoxicol. Environ. Saf. 106 (2014) 226–231.
[51] J.W. Lee, M. Kidder, B.R. Evans, S. Paik, A.C. Buchanan, C.T. Garten, R.C. Brown, Characterization of biochars produced from cornstovers for soil amendment, Environ. Sci. Technol. 44 (20) (2010) 7970–7974.
[52] J.H. Yuan, R.K. Xu, H. Zhang, The forms of alkalis in the biochar produced from crop residues at different temperatures, Bioresour. Technol. 102 (2011) 3488–3497.
[53] W. Ding, X. Dong, I.M. Ime, B. Gao, L. Ma, Pyrolytic temperatures impact lead sorption mechanisms by bagasse biochars, Chemosphere 105 (2014) 68–74.
[54] M. Ahmad, S.S. Lee, X. Dou, D. Mohan, J.K. Sung, J.E. Yang, Y.S. Ok, Effects of pyrolysis temperature on soybean stover- and peanut shell-derived biochar properties and TCE adsorption in water, Bioresour. Technol. 118 (2012) 536–544.
[55] X. Li, Q. Shen, D. Zhang, X. Mei, W. Ran, Y. Xu, G. Yu, Functional groups determine biochar properties (pH and EC) as studied by two-dimensional 13C NMR correlation spectroscopy, PLoS One 8 (6) (2013) e65949.
[56] K. Crombie, O. Mašek, S.P. Sohi, P. Brownsort, A. Cross, The effect of pyrolysis conditions on biochar stability as determined by three methods, GCB Bioenergy 5 (2013) 122–131.
[57] K. Crombie, O. Mašek, Investigating the potential for a self-sustaining slow pyrolysis system under varying operating conditions, Bioresour. Technol. 162 (2014) 148–156.
[58] K. Crombie, O. Mašek, Pyrolysis biochar systems, balance between bioenergy and carbon sequestration, GCB Bioenergy 7 (2) (2014) 349–361.
[59] W.K. Kim, T. Shim, Y.S. Kim, S. Hyun, C. Ryu, Y.K. Park, J. Jung, Characterization of cadmium removal from aqueous solution by biochar produced from a giant Miscanthus at different pyrolytic temperatures, Bioresour. Technol. 138 (2013) 266–270.
[60] O.R. Harvey, B.E. Herbert, R.D. Rhue, L. Kuo, Metal interactions at the biochar-water interface: energetics and structure-sorption relationships elucidated by flow adsorption microcalorimetry, Environ. Sci. Technol. 45 (13) (2011) 5550–5556.
[61] C. Cheng, J. Lehmann, J.E. Thies, S.D. Burton, M.H. Engelhard, Oxidation of black carbon by biotic and abiotic processes, Org. Geochem. 37 (2006) 1477–1488.
[62] Y. Chun, G. Sheng, C.T. Chiou, B. Xing, Compositions and sorptive properties of crop residue-derived chars, Environ. Sci. Technol. 38 (2004) 4649–4655.
[63] X. Chen, G. Chen, L. Chen, Y. Chen, J. Lehmann, M.B. McBride, A.G. Hay, Adsorption of copper and zinc by biochars produced from pyrolysis of hardwood and corn straw in aqueous solution, Bioresour. Technol. 102 (19) (2011) 8877–8884.
[64] O.R. Harvey, B.E. Herbert, R.D. Rhue, L. Kuo, Metal interactions at the biochar-water interface: energetics and structure-sorption relationships elucidated by flow adsorption microcalorimetry, Environ. Sci. Technol. 45 (13) (2011) 5550–5556.
[65] Z. Chen, B. Chen, D. Zhou, W. Chen, Bisolute sorption and thermodynamic behavior of organic pollutants to biomass-derived biochars at two pyrolytic temperatures, Environ. Sci. Technol. 46 (2012) 12476–12483.
[66] B. Chen, D. Zhou, L.Z. Zhu, Transitional adsorption and partition of nonpolar and polar aromatic contaminants by biochars of pine needles with different pyrolytic temperatures, Environ. Sci. Technol. 42 (14) (2008) 5137–5143.
[67] Z. Chen, B. Chen, C.T. Chiou, Fast and slow rates of naphthalene sorption to biochars produced at different temperatures, Environ. Sci. Technol. 46 (2012) 11104–11111.
[68] S.N. Guilhen, J. Coleti, J.A.S. Tenório, D.A. Fungaro, Influence of pyrolytic temperature on uranium adsorption capability by biochar derived from macauba coconut residue, Proceedings of the XIII Meeting on Nuclear Applications (ENAN), INAC 2017, Oct 22-27, Belo Horizonte, 2017.
[69] Y. Chen, H. Yang, X. Wang, S. Zhang, H. Chen, Biomass-based pyrolytic polygeneration system on cotton stalk pyrolysis: influence of temperature, Bioresour. Technol. 107 (2012) 411–418.
[70] G. Pilon, J.-M. Lavoie, Characterization of switchgrass char produced in torrefaction and pyrolysis conditions, BioResour 6 (2011) 4824–4839.
[71] M. Uchimiya, A. Orlov, G. Ramakrishnan, K. Sistani, In situ and ex situ spectroscopic monitoring of biochar's surface functional groups, J. Anal. Appl. Pyrol. 102 (2013) 53–59.
[72] Z. Yi, J. Yao, M. Zhu, H. Chen, F. Wang, Z. Yuan, X. Liu, Batch study of uranium biosorption by *Elodea Canadensis* biomass, J. Radioanal. Nucl. Chem. 310 (2016) 505–513.
[73] A.V. Naumkin, A. Kraut-Vass, S.W. Gaarenstroom, C.J. Powell, NIST X-Ray Photoelectron Spectroscopy Database [Internet], (2000) Available from: https://srdata.nist.gov/xps/Default.aspx , Accessed date: 14 June 2018.
[74] M.O. Krause, R.G. Haire, O. Keski-Rahkonen, J.R. Peterson, Photoelectron spectrometry of the actinides from Ac to Es, J. Electron. Spectrosc. Relat. Phenom. 47 (1988) 215–226.
[75] K. Winer, C.A. Colmenares, R.L. Smith, F. Wooten, Interaction of water vapor with clean and oxygen-covered uranium surfaces, Surf. Sci. 183 (1981) 67–99.
[76] Y.A. Teterin, V.M. Kulakov, A.S. Baev, N.B. Nevzorov, I.V. Melnikov, V.A. Streltsov, L.G. Mashirov, D.N. Suglobov, A.G. Zelenkov, A study of synthetic and natural uranium oxides by X-ray photoelectron spectroscopy, Phys. Chem. Miner. 7 (1981) 151–158.